



Statistical Shape Model of the Calcaneus Bone for Comprehensive Assessment of Three-Dimensional Morphology

Jie He¹, Zhexiao Guo², Yongjin Zhou³, Xiuyun Su^{1,*}, Guoxian Pei^{1,*}

¹Southern University of Science and Technology Hospital, Shenzhen, China

²Department of Chinese and Bilingual Studies, The Hong Kong Polytechnic University, Hongkong, China

³Health Science Center of Biomedical Engineering, Shenzhen University, Shenzhen, China

Email address:

yjzhou@szu.edu.cn (Yongjin Zhou), suxiuyun@sustech-hospital.com (Xiuyun Su), nfperry@163.com (Guoxian Pei)

*Corresponding author

To cite this article:

Jie He, Zhexiao Guo, Yongjin Zhou, Xiuyun Su, Guoxian Pei. Statistical Shape Model of the Calcaneus Bone for Comprehensive Assessment of Three-Dimensional Morphology. *International Journal of Biomedical Science and Engineering*. Vol. 11, No. 2, 2023, pp. 27-32.

doi: 10.11648/j.ijbse.20231102.12

Received: August 1, 2023; **Accepted:** August 23, 2023; **Published:** August 28, 2023

Abstract: Calcaneus is the most susceptible tarsal bone to fractures, presenting the most challenging treatment for associated tissue damage. Intra-articular calcaneal fractures present substantial challenges for patients and surgeons due to their association with both immediate and delayed complications. The purposes of this study were to establish a method for three dimensional morphological measurements of the normal calcaneus, we develop a statistical shape model (SSM) of the calcaneus that incorporates CT scans to enable a comprehensive assessment of its three-dimensional morphology. Though surface-based registration and point-wise correspondence analysis, the left and right calcaneus bones were compared with a variety of shape analysis. The compactness and parallel analysis test on the statistical shape model yielded 7 prominent shape modes of variations (MoVs), which accounted for approximately 89% of the total 3D variations in the population of shapes. Among these modes, two captured discriminating features from both the left and right calcaneus bones (p value < 0.05). Visual inspection confirmed that these two shape modes represented abnormalities in the anterior and anteromedial parts of the calcaneus, highlighting them as the primary bony risk factors in ankle injuries. In conclusion, our study utilizing a Statistical Shape Model (SSM) has identified significant shape variations (MoVs) of the calcaneus bone which correlate significantly with the left and right sides of the body. The results of our study also demonstrate the potential utility of the SSM as a tool for providing guidance in surgical planning and treatment of calcaneus pathologies.

Keywords: Calcaneus, Statistical Shape Model (SSM), Morphology

1. Introduction

Calcaneal fractures are the most common type of tarsal bone fracture and associated with a high degree of morbidity and disability, accounting for about 2% of all fractures and 60% of tarsal bone fractures, with approximately 75% of these fractures being intra-articular [1]. Effective surgical planning and method selection often necessitate a thorough understanding of the shape and morphological features of the target object. Calcaneus fractures account for approximately 2% of all human bone fractures and can result in long-term

discomfort and disability for patients. As the largest tarsal bone, the calcaneus plays a crucial role in stabilizing the human body, and any pathologies affecting this bone can significantly impact mobility and quality of life [2-4].

To evaluate calcaneus fractures and determine the efficacy of treatment, three imaging techniques are typically employed: X-ray, CT, and MRI [3, 5, 6]. Among these, CT imaging is currently considered the gold standard for diagnostics due to its ability to reconstruct the scanned object, which is an invaluable advantage [5-7]. Morphological measurements of the calcaneus have predominantly been limited to the two-dimensional (2D) plane and have been

obtained through various methods, including anatomical measurements of cadavers, X-rays, CT scans, and 3D reconstruction images using a hospital graphics workstation [8-10]. Although these methods yield accurate results, obtaining cadaver specimens can be challenging. Aleksandra et al [11]. developed a morphometric and anatomically accurate statistical shape model of calcaneus based on computed tomography, to achieve pre-operative planning and treatment of calcaneus fractures for future implant procedures. Nicola et al [12]. employed statistical shape model to evaluate three-dimensional shape variation using weightbearing computed tomography (WBCT) data of asymptomatic healthy individuals, which shows a promise for clinical evaluation of the subtalar joint. Amy et al [13]. applied computational morphometrics to quantify anatomical variation and congruency of the talocrural joint that revealed inter-individual morphometric differences at the articular regions. Early studies utilizing WB primarily focused on the tibiotalar articular regions to establish joint space distance relationships of the ankle joint [14-16]. Additionally, the analysis of joint space in previous studies lacked the assessment of bone morphology variation, articular coverage, and congruency of mated articular surfaces within the ankle joint. Therefore, enhancing our comprehension of ankle joint morphometrics is vital for the ongoing advancement of surgical treatment strategies. Statistical shape model offers a powerful tool for visualizing and analyzing 3D morphological differences [17-20]. By utilizing correspondence particles, statistical shape model allows for the identification of mean bone shapes and shape modes of variation, effectively eliminating human bias. However, previous studies applying SSM in the foot and ankle have primarily focused on assessing bone variation independently of joint relationships.

To establish a calcaneus statistical shape model, it is necessary to more comprehensively characterize the shape of the calcaneus by accurately measuring the anatomical parameters of the calcaneus and utilizing a deep fusion model. The aim of this study was to create a calcaneus statistical shape model that incorporates cone-beam whole-body computed tomography scans. This SSM would enable the assessment of shape variances and provide a comprehensive description of the healthy calcaneus joint's three-dimensional morphology. In clinical trials, we will focus on an efficiency framework for treatment in ankle or hindfoot pathologies.

2. Methods

2.1. Manual Annotations

Retrospective CT data from hospital records have been used in this study. Initially, 82 CT scans of healthy subjects aged 18–80 years were collected from Southern University of Science and Technology Hospital. A set of 512×512 images was included, and slice thickness ranged from 0.450–1.250 mm, saved in DICOM format. All calcaneus CT scans were screened by a radiologist to confirm the absence of any

known foot pathology in the scanned foot. A total of 82 subjects contributed volume data for 41 left and 41 right feet. The calcaneus was first segmented from the hindfoot by setting the threshold in Mimics 19.0 to 266 HU. The segmented regions were reconstructed to acquire the 3D morphologies of the calcaneus separated from the surrounding tissue. To achieve high-quality surfaces in the geometric model, we smoothed and adjusted 82 reconstructed talus models to a smoothing degree of 0.8 mm. After saving the 3D objects in STL format on Mimics, it was translated to NIFTI images (nii format) using Slicer for training. The calcaneus CT datasets were first converted into NIFTI images using Python. Additionally, the datasets were manually segmented slice by slice in Slicer 5.0.3 by orthopedists, who evaluated the segmentation results in follow-up, as depicted in Figure 1.

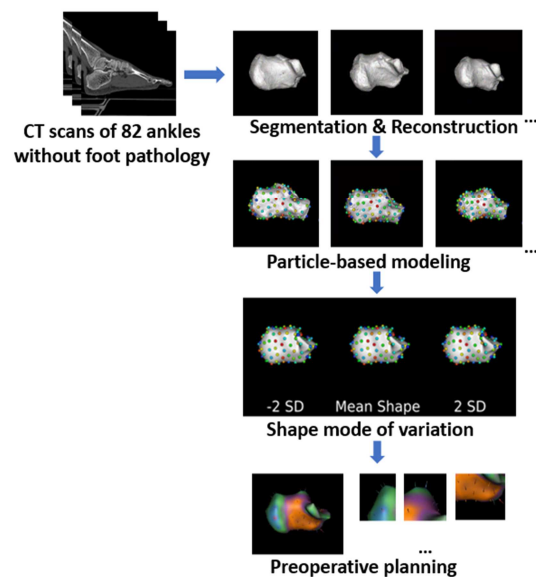


Figure 1. The framework of our method.

2.2. Segmentation of Calcaneus

The calcaneus bones were segmented in three dimensions from each CT scan using commercial segmentation software (Mimics 20; Materialise). The semi-automatic segmentation process involved steps such as thresholding, bone labeling, region growing, hole filling inside segmentation masks, and smoothing, and other relevant steps. The extracted triangulated bone surfaces from the segmentation results were exported as volumetric meshes using the same software. Overall, the dataset consisted of 82 bone surface shapes, and a subset of shapes was utilized to generate the statistical shape model of the calcaneus bones in later steps.

2.3. Extraction of Calcaneus Features and Evaluation

The covariance matrix was computed for the data vectors containing ordered coordinates of corresponding points across all calcaneus shapes. Principal component analysis (PCA) was then applied to the covariance function, yielding shape modes of variations (MoVs) that indicate the direction

of change. The quality of the resulting shape model was assessed using four established evaluation tests. The generality test assessed the model's ability to represent unseen shapes from the same class as the training set. Conversely, the specificity test evaluated whether any generated shape belonged to the same class as the training set. The compactness test measured the amount of variability captured within each mode of variation, which aimed to quantify the model's compactness. The algorithm for these tests is presented in Table 1. The reconstruction error, which represents the distance between two shapes, was computed by averaging the absolute distances between all pairs of corresponding points on the two surfaces, following the method described by Styner *et al.* [21].

Table 1. Algorithm of generality evaluating the performance of model.

| |
|--|
| 1: For each sample in x_i dataset |
| 1.1: take x_i out as the test sample |
| 1.2: generate shape model using all other samples |
| 1.3: reconstruct x_i using the first M shape modes of model ($1 \leq M \leq \text{rank}$ of model) and call reconstructed shape $x_i'(M)$ |
| 1.4: calculate distance between x_i and $x_i'(M)$ |
| 2: Based on the distances of average to calculate G(M) |
| $G(M) = \frac{1}{N} \sum_1^N D(x_i, x_i'(M))^2$ |

Table 2. Algorithm of compactness evaluating the performance of model.

| |
|---|
| 1: For each shape mode M of the model ($1 \leq M \leq \text{rank}$ of model) |
| 1.1: calculate the sum of variance by first M eigenvalues |
| $G(M) = \frac{1}{\sum \lambda} \sum_1^M \lambda_i$ |

Table 3. Algorithm of specificity evaluating the performance of model.

| |
|--|
| 1: Repeat this experiment for M between 1 and rank of the model |
| 1.1: sample a new shape using the first M shape modes of the model ($1 \leq M \leq \text{rank}$ of model) and call it $x_i'(M)$ |
| 1.2: calculate distance of $x_i'(M)$ |
| 1.3: to all shapes in the dataset and call the closest shape x_i |
| 2: Based on the distances of average to calculate S(M) |
| $S(M) = \frac{1}{N} \sum_1^N D(x_i'(M), x_i)$ |

3. Results

We generated the statistical shape model (SSM) for the talus using the group of 82 shapes as a training set, following the steps outlined in the methods section. The results of the generality test demonstrate that increasing the number of shape modes improves the accuracy of shape reconstruction.

With the inclusion of approximately 95% of the data variance and around 15 shape modes, the surface reconstruction error below the average resolution of the CT images. The compact shape model is a model capable of accurately reconstructing new shape instances using a insignificant number of shape parameters. In light of the varying influence of bone size on the overall population variance, particularly in larger bones like the calcaneus, the dominance of size was quantified as the percentage of variance explained by the first principal component. To assess the data variance captured by the model, the compactness test quantifies the increase in the amount of captured variance with an increasing number of principal components. The compactness chart includes eigenvalues obtained from a simulated dataset, as well as a Scree plot generated by parallel analysis. The smaller generalization error indicates a better statistical shape model, and model is considered to have population coverage when further increasing the number of training samples no longer enhances its generality ability. When the number of models increased to 15, the Generality results were already below 1.5, indicating good generalization ability of our model, as shown in Figure 3.

Based on the eigenvalues obtained from parallel analysis, the first 7 shape modes were identified as the most statistical significant nonspurious shape variations. These 7 modes collectively account for approximately 89% of the total shape variations. The captured amount of shape variation by each mode, along with the corresponding p-values from t-tests comparing the left and right calcaneus bones, are presented in Table 4.

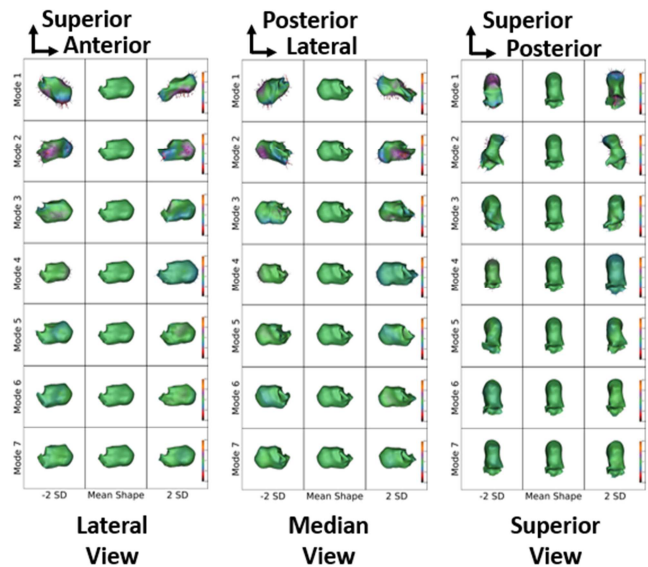


Figure 2. Calcaneus bone of subjects in three view.

Table 4. Algorithm of generality evaluating the performance of model.

| | Mode |
|------------|-------|-------|-------|-------|-------|-------|-------|
| Eigenvalue | 1 | 2 | 3 | 4 | 5 | 6 | 7 |
| P value | 38.1% | 27.5% | 9.5% | 7.1% | 2.9% | 2.4% | 1.5% |
| | 0.376 | 0.001 | 0.885 | 0.842 | 0.001 | 0.668 | 0.974 |

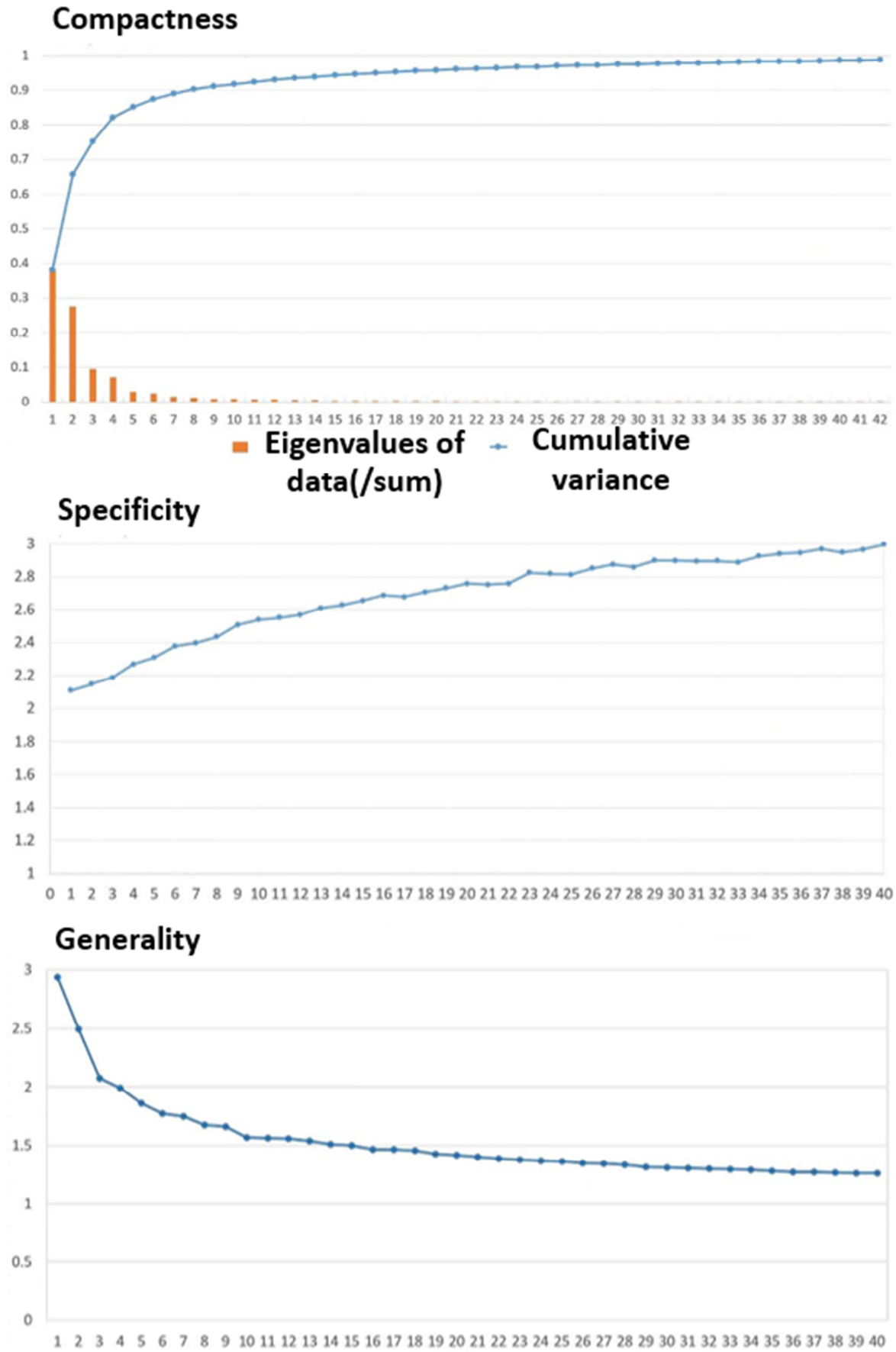


Figure 3. Statistic shape model evaluation results.

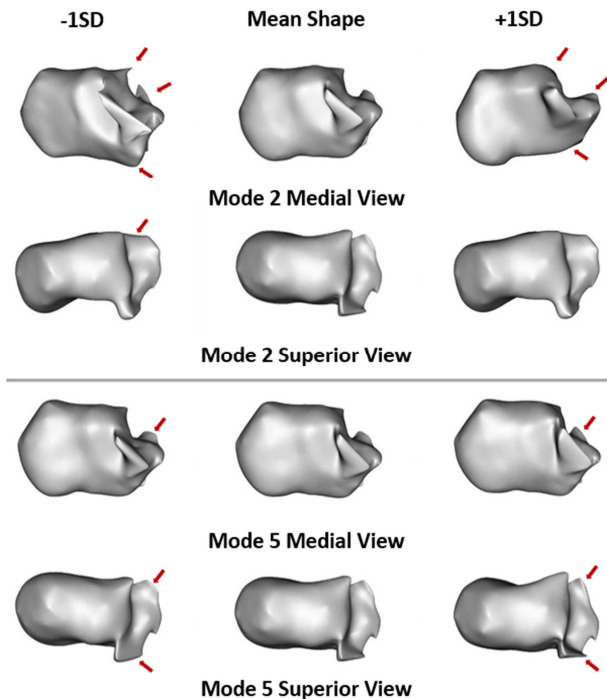


Figure 4. Visualize bone shape variations for the second and fifth modes of variation. Red arrows show the areas that are mainly affected in each modes of variation.

As table 4 reveals that the shape modes most strongly associated with differences between the left and right calcaneus are Modes 2 and 5. Therefore, we focus the remainder of our analysis on the two primary discriminating shape modes. The two prominent shape modes (Modes 2 and 5), explained the following changes (Figure 4): mode 2 variations mainly in anterior part and also in anteromedial part of the calcaneus, mode 5 variations mainly in the anterolateral process of the calcaneus.

4. Conclusion

The construction of an anatomically accurate statistical shape model of the calcaneus necessitates close collaboration between image processing engineers, radiologists, and orthopedic surgeons. The proposed statistical shape model includes a mathematically quantified shape description of the calcaneus, which can be used to analyze expected shape information and diagnose pathological changes. Our study aimed to compare the shape of the calcaneus bone between left and right groups, using a 3D Statistical Shape Model. A sample of healthy adults underwent 3D imaging of their calcaneus bones using a Statistical Shape Model. The left and right calcaneus bones were compared using a variety of shape analysis techniques, including surface-based registration and point-wise correspondence analysis. This enabled a quantitative characterization of the intricate 3D geometry of the bone in relation to shape variation modes, as well as the identification of specific modes exhibiting significant correlation between the left and right calcaneus

bones within the population.

We assessed the generality, specificity, and compactness of the SSM, the result in this study is nearly consistent with previous studies. Jinke Wang et al applied a proposed deformable surface model to construct a statistical shape model of the femur, and demonstrated its accuracy and efficiency. Their method achieved a compactness value of 1.38, and showed a generalization ability of 0.84 mm and a specificity of 1.52 mm. Since their dataset only included 10 individuals from public dataset, the reported results tended towards idealized values. Also the results reported by E. A. Audenaert and co-workers, they concluded that a minimum of 200 training samples is required to achieve sufficient population coverage [22]. Due to the dataset size of less than 200 samples in our study, the specificity results were not ideal. SSM provides us with a quantitative method for describing the overall shape of the calcaneus and detecting physiological differences between the left and right calcaneus, without depending on on a set of predefined measures that require laborious manual work. The results of models 2 and 5 reveal anatomical differences between the left and right calcaneal groups, indicating that there are differences in calcaneal morphology between the left and right feet, particularly in the anatomy of the anterior part of the bone. The color maps and deformation fields presented in the result illustrate the differences in shape between the left and right calcaneus, providing reference information for morphological changes in ankle surgery planning. Limitations of this study warrant discussion, it has two main limitations. Firstly, differences in voxel sizes of the input images may result in the omission of small anatomical details in images with larger voxel sizes. Secondly, the small dataset is a limitation. Although evaluation metrics were employed to evaluate the adequacy of the training shapes in terms of generality and specificity, the limited dataset size may result in overlooked biases and anatomical features. A larger cohort of subjects could unveil additional insights and address these limitations.

In conclusion, this study demonstrates the practicability of using 3D SSM to analyze patterns of shape changes between the left and right calcaneus, identify differences in two shape modes of the bone, and quantitatively characterize calcaneal-specific 3D shape variations. These findings highlight the value of SSM performed on CT scans for identifying and characterizing 3D potential bone deformities related to the ankle joint. In the future work, we will focus on evaluating the statistical shape model for analyzing the morphological changes of the calcaneus after fractures. This suggests that the framework could be used for early prevention of ankle diseases.

Acknowledgements

This project is supported by the Scientific Research Project of Southern university of science and technology hospital (2021-D9). Jie He and Zhexiao Guo contributed equally.

References

- [1] ESSEX-LOPRESTI P, PELTIER L F J C O, RESEARCH® R. The mechanism, reduction technique, and results in fractures of the os calcis [J]. 1993, 290: 3-16.
- [2] ALLEGRA P R, RIVERA S, DESAI S S, et al. Intra-articular calcaneus fractures: current concepts review [J]. 2020, 5 (3): 2473011420927334.
- [3] SPIERINGS K E, MIN M, NOOIJEN L E, et al. Managing the open calcaneal fracture: A systematic review [J]. 2019, 25 (6): 707-13.
- [4] VOSOUGHI A R, BORAZJANI R, GHASEMI N, et al. Different types and epidemiological patterns of calcaneal fractures based on reviewing CT images of 957 fractures [J]. 2022, 28 (1): 88-92.
- [5] PRANATA Y D, WANG K-C, WANG J-C, et al. Deep learning and SURF for automated classification and detection of calcaneus fractures in CT images [J]. 2019, 171: 27-37.
- [6] RAHMANIAR W, WANG W-J J A S. Real-time automated segmentation and classification of calcaneal fractures in CT images [J]. 2019, 9 (15): 3011.
- [7] BOOZ C, NÖSKE J, ALBRECHT M H, et al. Traumatic bone marrow edema of the calcaneus: evaluation of color-coded virtual non-calcium dual-energy CT in a multi-reader diagnostic accuracy study [J]. 2019, 118: 207-14.
- [8] SCHMUTZ B, LÜTHI M, SCHMUTZ-LEONG Y K, et al. Morphological analysis of Gissane's angle utilising a statistical shape model of the calcaneus [J]. 2021, 141: 937-45.
- [9] QIANG M, ZHANG K, CHEN Y, et al. Computer-assisted virtual surgical technology in pre-operative design for the reconstruction of calcaneal fracture malunion [J]. 2019, 43: 1669-77.
- [10] ARENA C B, SRIPANICH Y, LEAKE R, et al. Assessment of hindfoot alignment comparing weightbearing radiography to weightbearing computed tomography [J]. 2021, 42 (11): 1482-90.
- [11] MELINSKA A U, ROMASZKIEWICZ P, WAGEL J, et al. Statistical, morphometric, anatomical shape model (atlas) of calcaneus [J]. 2015, 10 (8): e0134603.
- [12] KRÄHENBÜHL N, LENZ A L, LISONBEE R J, et al. Morphologic analysis of the subtalar joint using statistical shape modeling [J]. 2020, 38 (12): 2625-33.
- [13] LENZ A L, KRÄHENBÜHL N, PETERSON A C, et al. Statistical shape modeling of the talocrural joint using a hybrid multi-articulation joint approach [J]. 2021, 11 (1): 7314.
- [14] WILLEY M C, COMPTON J T, MARSH J L, et al. Weight-bearing CT scan after tibial pilon fracture demonstrates significant early joint-space narrowing [J]. 2020, 102 (9): 796-803.
- [15] PAVANI C, BELVEDERE C, ORTOLANI M, et al. 3D measurement techniques for the hindfoot alignment angle from weight-bearing CT in a clinical population [J]. 2022, 12 (1): 16900.
- [16] RICHTER M, DUERR F, SCHILKE R, et al. Semi-automatic software-based 3D-angular measurement for Weight-Bearing CT (WBCT) in the foot provides different angles than measurement by hand [J]. 2022, 28 (7): 919-27.
- [17] FLISS B, LUETHI M, FUERNSTAHL P, et al. CT-based sex estimation on human femora using statistical shape modeling [J]. 2019, 169 (2): 279-86.
- [18] BAHL J S, ZHANG J, KILLEN B A, et al. Statistical shape modelling versus linear scaling: effects on predictions of hip joint centre location and muscle moment arms in people with hip osteoarthritis [J]. 2019, 85: 164-72.
- [19] KASTEN Y, DOKTOFSKY D, KOVLER I. End-to-end convolutional neural network for 3D reconstruction of knee bones from bi-planar X-ray images; proceedings of the Machine Learning for Medical Image Reconstruction: Third International Workshop, MLMIR 2020, Held in Conjunction with MICCAI 2020, Lima, Peru, October 8, 2020, Proceedings 3, F, 2020 [C]. Springer.
- [20] FUESSINGER M A, SCHWARZ S, NEUBAUER J, et al. Virtual reconstruction of bilateral midfacial defects by using statistical shape modeling [J]. 2019, 47 (7): 1054-9.
- [21] STYNER M A, RAJAMANI K T, NOLTE L-P, et al. Evaluation of 3D correspondence methods for model building; proceedings of the Information Processing in Medical Imaging: 18th International Conference, IPMI 2003, Ambleside, UK, July 20-25, 2003 Proceedings 18, F, 2003 [C]. Springer.
- [22] AUDENAERT E A, PATTYN C, STEENACKERS G, et al. Statistical shape modeling of skeletal anatomy for sex discrimination: their training size, sexual dimorphism, and asymmetry [J]. 2019, 7: 302.